Structural Characterization of Azurin from *Pseudomonas aeruginosa* and Some of Its Methionine-121 Mutants†

Loretta M. Murphy,‡ Richard W. Strange,‡ B. Göran Karlsson,§ Lennart G. Lundberg,§ Torbjörn Pascher,§ Bengt Reinhammar,§ and S. Samar Hasnain*,‡

Molecular Biophysics Group, Daresbury Laboratory, Warrington WA4 4AD, Cheshire, U.K., and Department of Biochemistry and Biophysics, Chalmers University of Technology and University of Göteborg, S-412 96 Göteborg, Sweden

Received August 3, 1992; Revised Manuscript Received November 23, 1992

ABSTRACT: Azurin from *Pseudomonas aeruginosa* and two mutants where the methionine ligand has been mutated have been studied in order to directly investigate the functional and structural significance of this ligand in the blue copper proteins. Reduction potentials, X-ray absorption fine structure (XAFS), electron paramagnetic resonance (EPR), and optical spectra are obtained in an attempt to provide a direct correlation between the spectrochemical properties and the immediate structure of this redox center.

Azurin from *Pseudomonas aeruginosa* (Az_p) is a member of a family of functionally related metalloproteins, known as blue copper proteins, which mediate electron transfer (Ryden, 1984). Az_p is a monomeric protein of molecular mass 14 600 Da and contains one type 1 copper center. Type 1 copper centers are characterized by their electronic absorption spectrum (a very high intensity band centered at ca. 600 nm), electron paramagnetic resonance (EPR) spectrum (they possess a small hyperfine splitting in the $g_\parallel$ region), and a high reduction potential (184–785 mV) (Adman, 1985, 1991; Reinhammar, 1979).

The three-dimensional structure of Az_p has been reported both at medium resolution (Adman et al., 1978, 1981) and very recently at high resolution, for the recombinant wild-type protein (Nar et al., 1991). The coordination sphere around copper consists of two nitrogens (residues His-117 and His-46), two sulfur donors (residues Cys-112 and Met-121), and an oxygen (residue Gly-45) arranged in a distorted trigonal bipyramid. X-ray crystallographic studies on other blue proteins, such as plastocyanin from poplar leaves (Pc_p) (Guss & Freeman, 1983; Guss et al., 1986), plastocyanin from algae (Collyer et al., 1990), and azurin from *Alcaligenes denitrificans* (Az_a) (Baker, 1988; Norris et al., 1986), show a very close similarity at the Cu site. In particular, the position of His and Cys has been found to be highly conserved. In each of these proteins a fourth ligand is identified as a weakly coordinated methionine residue. From these studies, it would appear that the minimum requisite for a blue Cu site is four ligands, but the fourth ligand may not necessarily be a methionine, since stellacyanin from Japanese lacquer tree (St) exhibits all the characteristic spectrochemical properties of a type 1 site but does not contain any methionine residues (Bergman et al., 1977).

There is considerable interest in how the same basic framework, found for all structurally characterized small blue proteins, is fine tuned to give reduction potentials ranging from 184 (St) to 680 mV in rusticyanin (Ru) from *Thiobacillus ferro-oxidans*. In particular, the role of methionine (or another fourth ligand) has been extensively discussed in terms of fine tuning the reduction potential (Gray & Malmström, 1983; Guss et al., 1986). To address this directly, we have undertaken an investigation of the structure–function relationship through site mutations of methionine in Az_p. We have used a variety of physical techniques which are able to examine the Cu center directly, including X-ray absorption fine structure (XAFS), optical spectroscopy, and EPR. Reduction potential measurements have also been made. Results are presented on two mutants. In one case the methionine-121 amino acid residue has been replaced by an aspartate, to give a mutant protein subsequently referred to as Asp-121; in the second, the amino acid residues from methionine-121 to lysine-128 in the native protein have been deleted to produce a mutant azurin subsequently referred to as End-121.

MATERIALS AND METHODS

Materials. All chemicals were reagent grade and used without further purification. Water was deionized using a Elgastat water treatment system. The buffer systems used for the experiments were 10 mM *N*-(2-hydroxyethyl)-piperazine-*N'*-2-ethanesulfonic acid (HEPES), pH 8.0, except for End-121 where pH 7.0 was used, and 10 mM 2-(*N*-morpholino)ethanesulfonic acid pH 5.0. All protein manipulations were performed at 4 °C unless otherwise stated. All final stage concentrations were performed using Centricon-10 concentrators from Amicon Ltd.

Preparation of Native Azurin. Azurin was prepared from frozen *P. aeruginosa* cell paste using a modification of the method described by Parr et al. (1976). The only modification replaced the Sephadex G-75 column by a Sephacryl S100HR column. The spectral absorbence ratio A_{625}/A_{280} was 0.54.

Expression of Azurin and Site-Directed Mutagenesis of the Met-121 Residue. Az_p was expressed in *Escherichia coli* as described elsewhere (Karlsson et al., 1989, 1991). In the purification of the wild-type protein, an anionic exchange chromatography step was included (van de Kamp et al., 1990), and the absorbance ratio of the wild type was 0.61. In the purification of the mutant proteins, this step results in the loss of copper. The absorbence ratio of Asp-121 was 0.55 at pH 4, and that of End-121 was 0.18.

Electronic Absorption and EPR Spectroscopy. Electronic absorption spectra were recorded over the range 350–800 nm on a Phillips Series PU 8700 single-beam spectrometer or with a Shimadzu UV-3000 dual wavelength/double-beam spectrometer over the range 300–900 nm. EPR spectra were

† This work is supported by grants from the Swedish Natural Research Council and the Science and Engineering Research Council, U.K.

‡ Daresbury Laboratory.

§ Chalmers University of Technology and University of Göteborg.

0006-2960/93/0432-1965$04.00/0

recorded at X-band on a Varian E-3 spectrometer at 77 K or on a Bruker ER-200D-SRC spectrometer at 20 K. Simulated EPR spectra were produced with an in-house developed program using second-order perturbation theory.

Reduction Potentials Measurements. Reduction potentials were measured using the optically transparent thin layer electrode (OTTLE) technique described elsewhere (Heineman et al., 1975) with some modifications (Ellis, 1986). The temperature was measured with a copper–constantan thermocouple inserted into the OTTLE cell, and the temperature of the protein solution was kept within ±0.05 °C of the preset value with a thermostated cell holder. The potentiostat was constructed according to Urbaniczky (1984), and the optical measurements were performed in a Shimadzu UV-3000 spectrometer. Tris(1,10-phenanthroline)cobalt(III) perchlorate was used as a redox mediator. Both azurin and mediator had a concentration of 1 mM (Sailasuta et al., 1979). The buffer used was the same as for XAFS measurements except that KCl was added to a final concentration of 100 mM to improve the conductivity. All measurements were made at 25 °C.

X-ray Absorption Spectroscopy. All protein samples were concentrated to a volume of ca. 0.25 mL to give copper concentrations in the range 2–7 mM. The samples were placed in Perspex XAFS cells, with Mylar windows, and frozen in liquid nitrogen. The XAFS cell window dimensions were 8 × 10 × 2mm (height × width × depth). XAFS data was recorded at the Cu K-edge on Wiggler station 9.2 operating in the fluorescence mode at the Synchrotron Radiation Source (SRS), Daresbury Laboratory, U.K. The SRS was operating at an energy of 2.0 GeV with an average current of 150 mA and beam lifetime in excess of 20 h. An order sorting Si(220) double-crystal monochromator was used to reduce harmonic contamination in the monochromatic beam. For extended X-ray absorption fine structures (EXAFS) data collection, a beam size of 3 × 5 mm (height × length) was used; this was reduced to a height of 0.75 mm for X-ray absorption near edge structures (XANES) data collection. All protein samples were cooled to 77 K through the use of a liquid nitrogen cryostat. A 13-element germanium solid-state detection system was employed, allowing higher quality fluorescence XAFS data to be recorded than published previously (Groeneveld et al., 1986; Tullius et al., 1978), where scintillation detectors with a metal foil were used for detecting the X-ray fluorescence and for discriminating X-ray scatter from the sample. The X-ray energy was calibrated by measuring the edge spectrum of Cu foil in transmission mode and setting the first inflection point at 8982 eV.

An average of 12 scans were recorded per sample. For each sample the individual scans were examined, and each detector element was reweighted relative to the edge height and then summed using the Daresbury EXCALIB program (Morrell et al., 1989). Background subtraction and normalization was performed using the Daresbury Laboratory program EXBACK (Morrell et al., 1989).

The Daresbury Laboratory program EXCURV92 (Binsted et al., 1991, 1992) was used for data analysis, employing fast curved wave single and multiple scattering theory (Gurman et al., 1984, 1986) on k^3-weighted EXAFS data. The Cu, N, C, and O phase shifts were calculated using the program MUFPOT and the S phase shift was obtained from EXCURV92, which uses a simplified version of the MUFPOT program. Details of the procedure used are given elsewhere (Binsted et al., 1987). The phase shifts have previously been used to fit a number of copper–histidine/pyridine model compounds (Strange et al., 1987; Blackburn et al., 1988). The photoelectron energy threshold value, E_0, was treated as a single overall parameter for the multiple-shell fit. This has been found adequate for systems where the back-scatterers are all of a similar nature. The quality of the theoretical simulations was determined by a visual comparison of the EXAFS and Fourier transforms and by the fit index (FI) and R factor (R) as described in Binsted et al. (1992). The use of constrained refinement procedures (Hasnain et al., 1988; Binsted et al., 1992) was made to reduce the number of free parameters in the least-squares refinement.

RESULTS

Optical Absorption Spectroscopy. Figure 1a shows the visible spectra at pH 8.0 for the oxidised Az_p and mutants. For comparison, data for St at pH 7.0 are included. In all the mutants, a strong absorption band is observed at ~450 nm. A similar band is observed for St. Figure 1b shows the pH dependence on the absorbence of the Asp-121 mutant. The spectrum at low pH is similar to the Az_p spectrum. As the pH is increased, the absorption bands at ca. 780 and ca. 625 nm decrease while the band at ca. 450 nm increases markedly. There is an isosbestic point at ca. 365 nm and another at ca 520 nm. The blue band is shifted from 625 to ca. 615 nm. An apparent pK_a value of 6.2 was calculated from the changes in absorption of the 450-nm band and the changes in the EPR spectra with pH.

EPR Spectroscopy. Figure 2 shows the X-band EPR spectra at 77K of Az_p (pH 8.0), Asp-121 (pH 5.0 and 8.0) and End-121 (pH 7.0). The EPR spectrum of Az_p is typical of that found for small blue copper proteins, i.e., a narrow hyperfine splitting in the $g_\parallel$ region. Asp-121 and End-121 also exhibit small $A_\parallel$ values. However, in contrast to the axial spectrum observed for Az_p and Asp-121 at pH 5.0, both Asp-121 at pH 8.0 and End-121 pH 7.0 exhibit rhombic EPR spectra, similar to that found for St at pH 11 (also shown here for comparison). The EPR spectra were simulated using the parameters shown in Table I. The close similarity of Asp-121 at pH 5.0 to the wild type is evident from the EPR parameters, whereas the parameters for Asp-121 at pH 8.0 are similar to those obtained for End-121 and St. We note that g_x is decreased by 0.010–0.015 in going from Az_p to St, End-121, and Asp-121 (pH 8.0), while g_y and g_z increase by 0.030 and 0.020, respectively, with the hyperfine coupling constant A_x increasing by about 7-fold and A_z reducing by approximately half.

Reduction Potential Measurements. The reduction potential ($E_{m,8}$) for the wild type was determined as 293 mV (Table II). The titrations of the mutants are more complex than that of the wild type. During a cycle of two titrations, starting with oxidized protein and reducing it and then oxidizing it again, the mutants lose approximately 30% of the copper absorption at 625 nm compared to the wild type, which loses less than 1%. In the time scale of the redox experiment (6 h) the oxidized forms of the azurin mutants are stable, so it must be the reduced forms that lose copper. The decrease in absorption continues with further titration cycles. This means that it cannot be fast equilibrium between reduced and apoazurin. The reduction potentials for Asp-121 ($E_{m,8}$) and End-121 ($E_{m,7}$) were determined as 287 and 205 mV, respectively. The potentials were calculated as the mean of four consecutive titrations, where the maximum deviation from the ideal Nernst slope of 59 mV were 8 and 27 mV, respectively. The problems with the slope is probably due to the loss of Cu(I).

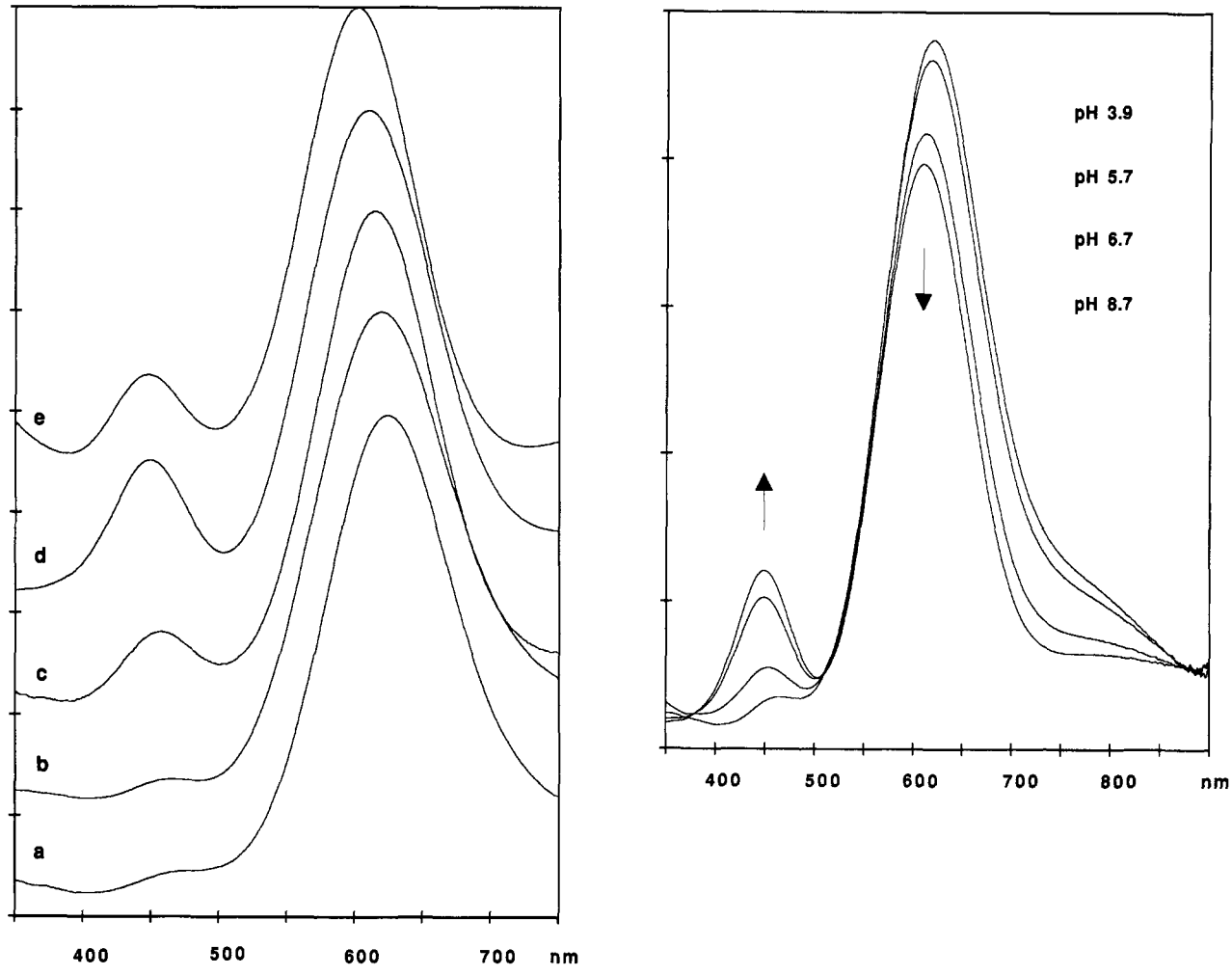

FIGURE 1: (a, left) Optical spectra for the oxidized forms of (a) Az_p (pH 8.0), (b) Asp-121 (pH 3.9), (c) Asp-121 (pH 7.0), and (d) End-121 (pH 7.0). For comparison, data for stellacyanin at pH 7.0 are included (e). (b, right) Optical absorption spectral changes of Asp-121 with pH between pH 3.9 and 8.7. Shifts of the ~450- and ~600-nm bands with increasing pH are indicated by the arrows.

XANES Data. Figure 3 shows the normalized absorption edge data for the oxidized protein samples. The spectra each exhibit a low-energy (8979 eV) feature typically associated with the Cu(II) oxidation state. This feature has been identified as originating from a 1s → 3d quadrupolar allowed transition (Schulman et al., 1976; Hahn et al., 1982). In addition to this, several other features are observed. The edge data for Az_p and Asp-121 at pH 5.0 both exhibit a similar slope in the absorption after the edge, between 9000 and 9025 eV. For Asp-121 at pH 8.0 and End-121, the absorption after the edge is more like that of stellacyanin. The XANES of the Az_p sample shows a more complex structure than the other proteins, thus reflecting differences in the coordination geometry of the ligands around the Cu.

EXAFS Data and Structural Interpretation. The Cu K-edge absorption spectrum of Az_p expressed in *E. coli* was found to be identical to that of Az_p isolated from *P. aeruginosa*. Figure 4 shows the EXAFS data for the oxidized Cu(II) form of the *E. coli* expressed azurin, Asp-121 (pH 5.0), Asp-121 (pH 8.0), and End-121. The close similarity between the spectra suggests that the primary coordination, due to the two histidines and the cysteine, is essentially the same for the three proteins. This similarity is reflected in the corresponding Fourier transforms which are shown in the lower panel of Figure 4. For example, the spectrum of the native protein and the spectra of the mutants are different in the second beat region between k = 5.5 and 6.5 Å^{-1}, as are the two mutant spectra between k = 4 and 5.5 Å^{-1}. These differences point toward small changes in the coordination sphere of the Cu atom when the Met-121 residue is replaced by aspartate or is deleted. Detailed analysis of the EXAFS data of the native azurin and of the End-121 and Asp-121 mutants is presented in the following section.

Analysis of Oxidized Azurin. The starting model for the EXAFS data analysis was based on the crystal structures of Az_p, which show an inner shell coordination for Cu(II) consisting of two histidine ligands (ca. 2.0–2.1 Å) and a cysteine ligand (ca. 2.1 Å) with additional ligands provided by sulfur from methionine (ca. 3 Å) and oxygen from a glycine residue (ca. 3 Å). The constrained refinement method involves treating the imidazole ring of a histidine ligand as a rigid unit during the least-squares analysis of the EXAFS data. In this case a single imidazole ring represents both of the coordinating histidines and its contribution to the EXAFS is doubled. This method results in a minimization of the number of independent parameters during refinement and offers the possibility of determining these parameters with some confidence. To further reduce the number of refinable parameters, the Debye–Waller parameters ($\alpha = 2\sigma^2$) of the C2/C5 and C3/N4 atoms [atom labeling as defined in Strange et al. (1987)] of the imidazole were refined together as a single variable. As a result, a total of eight independent parameters were refined: E_0, R_1, R_6, α_1, $\alpha_{2,5}$, $\alpha_{3,4}$, α_6, and the Cu–N1–C2 angle. Here, R_1 is the Cu–N1(His) distance and R_6 is the Cu–S(Cys)

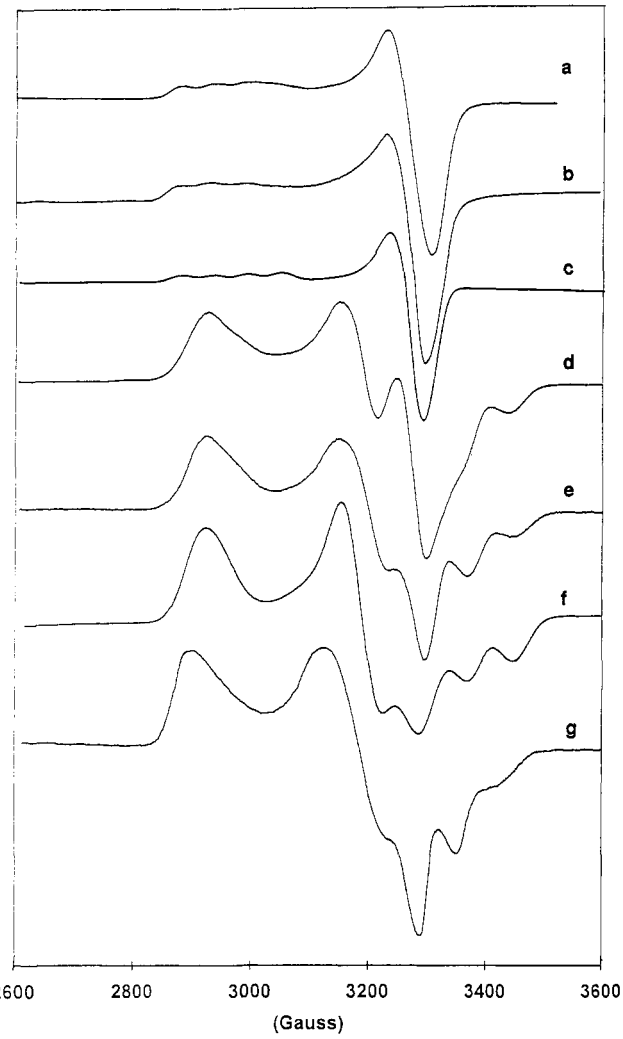

FIGURE 2: X-band EPR spectra of frozen solutions of (a) Az_p (pH 8.0), (b) Asp-121 (pH 5.0), (d) Asp-121 (pH 8.0), and (e) End-121 (pH 7.0). For comparison, data for St at pH 11.0 are also included (g). Example simulations for Asp-121 at pH 5.0 and 8.0 are shown in curves c and f, respectively.

Table I: EPR Parameters for Az_p (pH 5.2 and 9.2), End-121 (pH 7.0), Asp-121 (pH 5.0 and 8.0), and Stellacyanin (pH 1–9 and 11.0)[a]

protein	pH	g_x	g_y	g_z	A_x	A_z
Az_p[b]	9.2	2.035	2.051	2.276		51
Az_p[b]	5.2	2.035	2.052	2.263		56
Asp-121	5.0	2.035	2.055	2.260	10	56
Asp-121	8.0	2.020	2.085	2.295	76	21
End-121	7.0	2.025	2.085	2.295	76	21
St[c]	1–9	2.025	2.077	2.287	57	35
St[c]	11.0	2.025	2.089	2.312	73	<17

[a] The hyperfine couplings are given in units of 10^{-4} cm^{-1}. [b] Groenveld et al. (1987). [c] Malmström et al. (1970).

distance. Figure 5a shows the best constrained refinement simulation based upon two imidazole(His) and one S(Cys) using the curved wave multiple scattering theory. It is clear from Figure 5a that the primary contribution to the EXAFS between k = 3.6 and 12.5 $Å^{-1}$ has been taken into account by this basic model, which gives a FI = 0.35 and R = 20.9%. However, the lack of fit in the k range 4.5–8.0 $Å^{-1}$ of the EXAFS and also in the Fourier transform at 2.5–3.7 Å is obvious.

If the data for k = 3–3.6 $Å^{-1}$ are included in the analysis, then the presence of a low-Z scatterer at 2.23 Å (α = 0.016 $Å^2$) produces a significant improvement to the simulation.

Table II: Reduction Potentials for Az_p, Asp-121 (pH 5.0 and 8.0), End-121, and Stellacyanin

protein	E_m (mV) (pH 5.0)	E_m (mV) (pH 8.0)	E_m (mV) (pH 7.1)
Az_p	346	293	
Asp-121	327	287	
End-121			205
St[a]			184

[a] E_m was measured in 10 mM HEPES/0.1 M KCl at pH 8.0 and in 10 mM MES/0.1 M KCl, except for St (Reinhammar, 1972).

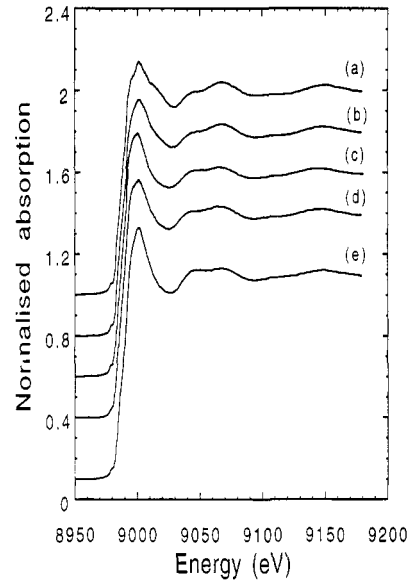

FIGURE 3: Normalized X-ray absorption near-edge structure (XANES) data for oxidized (a) Az_p (pH 8.0), (b) Asp-121 (pH 5.0), (c) Asp-121 (pH 8.0), and (d) End-121 (pH 7.0). For comparison, data for St at pH 11.0 are included (e).

There is no crystallographic evidence for a low-Z ligand at this distance in azurin. On the other hand, it is known that in the range k = 3–3.6 $Å^{-1}$ of the EXAFS spectrum, both data and simulation can be affected by the background subtraction, atomic contributions to the EXAFS, approximations in multiple scattering calculations, and the muffin-tin approximation of the atomic potentials used for calculating the atomic phase shifts. With the restricted data range, using k_{min} = 3.6 $Å^{-1}$, as presented here for all cases, the addition of a low-Z atom at ca. 2.26 Å in the native data and its subsequent refinement leads to a Debye–Waller factor of 0.05 $Å^2$ or higher, making no significant contribution to the EXAFS over this range. Thus, in view of the information available from crystallographic studies and the difficulty in extending the data to lower k, the short low-Z atom was rejected, and further refinement was carried out with the addition of a carbonyl O, associated with the glycine residue main chain, and a S from methionine. Addition of the O atom alone gave a minor improvement in the R factor (19.6%), with the oxygen refining to 2.79 Å (starting values used were 2.60 and 3.00 Å). Similarly, addition of the S(Met) alone, which refined to 3.45 Å (starting value 3.20 Å), only improved the fit to R = 19.4%. However, incorporation of both O and S together does lead to a significant improvement in the simulation, giving an R factor of 16.9% and a FI of 0.24. The better agreement with the experimental data compared with the basic model is apparent, reflecting the 30% decrease in FI.

However, it should be emphasized that it is possible to obtain a similar fit by assuming an alternative model. In particular, both the fit to the EXAFS and the lack of intensity in the Fourier transform between 3 and 3.5 Å can be accounted for

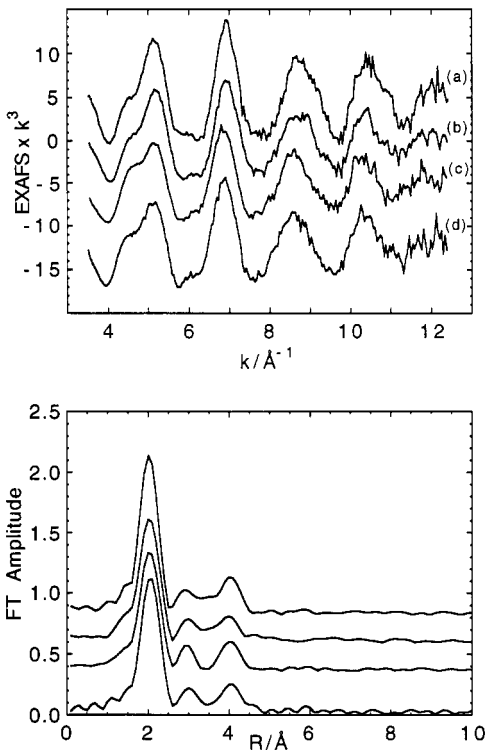

FIGURE 4: EXAFS data for the oxidized form of (a) Az_p (pH 8.0), (b) Asp-121 (pH 5.0), (c) Asp-121 (pH 8.0), and (d) End-121 (pH 7.0) with corresponding Fourier transforms shown in the lower panel. The Fourier transforms show that there are no significant contributions to the EXAFS data from shells > 5 Å from copper. The low amplitude at $R > 5$ Å in the Fourier transforms shows the high signal-to-noise ratio of the EXAFS data.

by including 2–3 carbon atoms at ca. 3.26 Å in place of the sulfur at 3.46 Å. Inclusion of two C atoms to the basic fit reduces the R factor from 20.5 to 18.9%. Addition of the S(Met) in the presence of these carbon atoms results in a best fit distance of 3.01 Å, with a FI = 0.25 and R = 17.5%. In this model the Cu–S(Met) distance comes close to the value obtained by crystallography. However, the fact that two satisfactory simulations of the data can be found for quite different Cu–S(Met) distances points to the difficulty, previously noted by several authors (Groeneveld et al., 1986; Tullius et al., 1978), of determining the position of the methionine contribution to the EXAFS of oxided Az_p. Similar effects have also been observed in the EXAFS of related structures, such as plastocyanin (Scott et al., 1982; Penner-Hahn et al., 1989) and amicyanin (Lommen et al., 1991). Indeed, a fit to the EXAFS data of native azurin can be obtained without the S(Met) contribution at all. A model which has the 2C shell at 3.26 Å and the 1O shell at 2.79 Å gives a FI = 0.24 and R = 16.9% (Table IIIb). The final simulation based on this model is shown in Figure 5b. We note that the possibility of carbon back-scatterers at 3.2–3.4 Å is consistent with the crystal structure for Az_p and related proteins (where they arise from the cysteine and histidine side chains, in fact there are more than two C atoms in this range, but only two carbons have been included due the large spread in distances displayed in the crystallographic structure). In each of these simulations, the total number of parameters refined was 12 and the number of independent data points was 17.8, thus from the point of view of refinement, the problem is well determined (Binsted et al., 1992). Simulations, where an O, a S, and two C are all included, are not any better than those obtained with one O and one S or one O and two C.

Analysis of the Mutant EXAFS Data. (A) End-121 Mutant. EXAFS data for the End-121 mutant was analyzed in the k range 3.6–11.2 Å^{-1}, with the starting model based on the above analysis, but where the S(Met) and the two C, possibly from the side chain, have been excluded. The simulation from the starting model (i.e., two imidazole + one S(Cys) + one O at 2.8 Å) resulted in a set of inconsistent Debye–Waller factors for the atoms of the imidazole rings. The two nitrogens in the first shell refined to an α_1 of 0.013 Å^2. This is about 150% of the value obtained for the second-shell carbon atoms of the imidazole ring ($\alpha_{2/5}$ = 0.007 Å^2) and is equal to the value obtained for the third-shell imidazole atoms ($\alpha_{3/4}$ = 0.013 Å^2). The simulation was therefore rejected as physically unrealistic. In any case, the value of α_1 is unusually large for a pair of low-Z back-scattering atoms coordinated at less than 2 Å. In addition, the higher R end of the first-shell peak in the Fourier transform indicated that a contribution at around 2.3 Å was not accounted for by the model and suggests a reinterpretation of the first-shell analysis. Detailed first-shell analysis of the raw EXAFS data was then attempted with several models. Some of the main results of this analysis are summarized in Table IVa which clearly demonstrate that two low-Z atoms (N) are required at ~1.9 Å, one S at ~2.1 Å and another low-Z ligand, possibly an oxygen, at ~2.3 Å. Models with only three atoms in the first shell show unacceptable behavior of the Debye–Waller terms for these atoms. Thus, the final model included four atoms in the first shell, two N from two histidines, one S, and another O at ~2.3 Å. The longer oxygen shell refined to 2.83 Å (α = 0.020 Å^2). Inclusion of the low-Z scatterer at 2.26 Å (α = 0.013 Å^2) lowers the Debye–Waller factor of the two nitrogens to 0.004 Å^2, similar to that found for the native protein, and gives a FI = 0.24 and R factor = 16.1%. A further 40% improvement in the FI results when the two C atoms are added and refined to 3.26 Å (FI = 0.14, R = 11.9%). The final simulation is shown in Figure 6, and the parameters are given in Table IVb.

(B) Asp-121 Mutant. The EXAFS and Fourier transforms for the Asp-121 mutants, measured at pH 5.0 and 8.0, are both similar to that of End-121. The analysis for each of these spectra was carried out using the same starting model as for End-121. Figure 7a shows the best simulation of the pH 8.0 spectrum resulting from this refinement. The first-shell coordination is like the end mutant in that a low-Z back-scatterer (at 2.23 Å) is required to fit the first shell in addition to the two N(His) at 1.93 Å, the S(Cys) at 2.16 Å, and one O at 2.88 Å. (FI = 0.28, R = 18.1%). Inclusion of two C atoms at 3.28 Å gave a reduction in FI of 25% (FI = 0.22, R = 14.8%; see Table Va).

Analysis of the Asp-121 EXAFS recorded at pH 5.0 resulted in a similar first-shell model of two N(His) at 1.93 Å, one S(Cys) at 2.15 Å, and one O at 2.26 Å. However, the longer oxygen shell (at 2.88 Å) refined to a Debye–Waller factor of 0.15 Å^2, compared with 0.023 Å^2 at pH 8.0. Thus, the simulation was identical when this shell was removed (FI = 0.30, R = 19.8%). If two C atoms at 3.26 Å are included in the simulation together with the 2.88-Å oxygen shell, then the α value for the oxygen is 0.05 Å^2, with a FI = 0.21 and R = 15.4% (Table Vb). The improvement in the FI is wholly due to the addition of the two C atoms, as may be seen if the oxygen is removed, then the FI is 0.22 and R = 16.1%.

DISCUSSION

The main structural parameters obtained from the EXAFS data of Az_p and the two mutants are summarized in Table VI

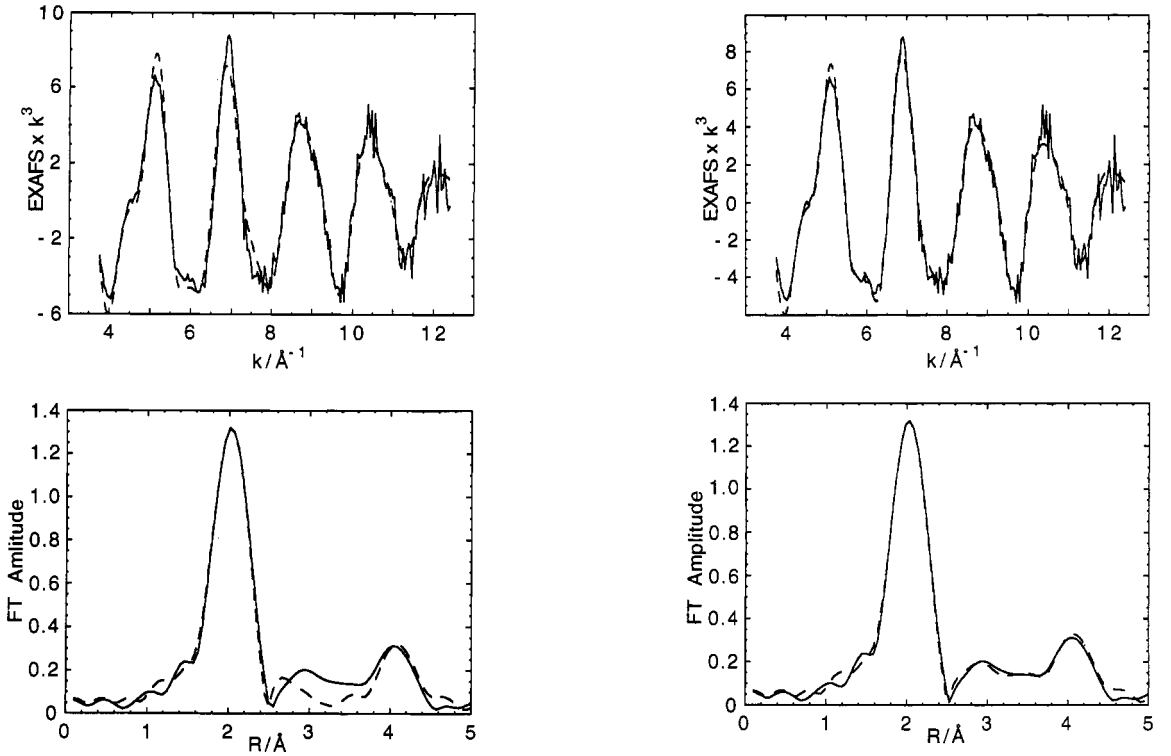

FIGURE 5: (a, left panels) Best constrained refinement simulation of Az_p based upon two imidazole(His) and one S(Cys) using the curved wave multiple scattering theory. (b, right panels) Constrained simulation obtained after incorporating both O from carbonyl at 2.79 Å and two C at 3.26 Å.

Table III: Structural Parameters for Oxidized Az_p at pH 8.0 Obtained with Different Simulation Models[a]

shell	atoms	R (Å)	$2\sigma^2$ (Å^2)	shell	atoms	R (Å)	$2\sigma^2$ (Å^2)
(a) Initial Model Used To Simulate Cu K-Edge EXAFS of Az_p[b]							
1	2N	1.92	0.005	4	2C	3.00	0.007
2	1S	2.12	0.000	5	2C	4.12	0.013
3	2C	2.90	0.007	6	2N	4.14	0.013
(b) Final Model Used To Simulate Cu K-Edge EXAFS of Az_p[c]							
1	2N	**1.92**	**0.005**	5	2C	4.12	**0.013**
2	1S	**2.12**	**0.000**	6	2N	4.14	0.013
3	2C	2.90	**0.007**	7	1O	**2.79**	**0.014**
4	2C	3.00	0.007	8	2C	**3.26**	**0.014**

[a] Section a lists basic 2N(His) + 1S(Cys) parameters, and section b lists final fit parameters with refined parameters given in bold. [b] E_o = 17.92; $2\sigma^2$ is the Debye–Waller factor; fit index = 0.35; R factor = 20.9%. [c] E_o = 17.92; $2\sigma^2$ is the Debye–Waller factor; fit index = 0.24, R factor = 16.9%.

along with the equivalent values from high resolution (<2 Å) crystallographic studies of Az_p, Az_a, and Pc_p. There is a resonable agreement between the two techniques. However, distances for histidines differ by nearly as much as the maximum coordinate error which may be expected in the crystallographic studies at these resolution. In EXAFS, an absolute accuracy of 0.02 Å is routinely achieved for the inner shell distances, as has been demonstrated by numerous studies of crystallographically characterized chemical systems by several groups [see, for example, Hasnain (1991)]. In the crystallographic studies of proteins, smaller errors than the observed differences would be expected because of the use of sophisticated refinement procedures. We note that similar differences have been observed for the histidine distance in the XAFS and crystallographic studies of single-crystal study of pseudoazurin (Adman, Hasnain, and Strange, unpublished results), thus the differences cannot be accounted for by the state of the sample. These differences have also been observed previously on Az_p and other blue copper proteins (Scott et al., 1982; Groenveld et al., 1986).

A comparison of the EXAFS distances in the Table VI shows that both the His and Cys ligands are at very slightly longer distances in the mutants compared to the native protein, consistent with a closer interaction with a fourth ligand. In particular, the increase in the Cu–S(Cys) distance by 0.03–0.04 Å would be expected to affect the overlap integral of the orbitals and is thus consistent with the optical spectral differences observed for the Asp-121 and End-121 mutants. The close spectral similarity of the End-121 mutant and the Asp-121 mutant at high pH is also reflected in the closeness of EXAFS parameters for the two.

The EXAFS analysis, however, does not provide any information about the origin of the oxygen shell at ~2.25 Å. Similarly, in the case of the two mutants, the origin of O shell at ~2.8 Å need not necessarily be the same as in the native protein, i.e., from the peptide of the Gly-45. We must therefore consider different possibilities in the assignment of these oxygen atoms. One possible assignment is that the oxygen shell at ~2.25 Å is from a water ligand. The copper coordination resulting from this assignment is shown schematically in Figure 8a,b for both mutants. A second proposal to be considered is that the short oxygen shell arises instead from a closer interaction of the Gly-45 oxygen with the copper atom. The copper site structure consistent with this proposal is shown schematically in Figure 8c,d. The relative merits of both of these models are discussed in detail below. We emphasis that the following discussion is based upon the assumption that only a minimal modification to the overall protein structure is required to accommodate the changes in the amino acid sequence when Met-121 is mutated.

The copper site in the wild-type blue proteins has been thought of as rigid and has been discussed in terms of a rack mechanism (Malmström, 1965). If the copper site is indeed rigid, then one may assume that the distance between the

Table IV: Parameters for EXAFS Analysis

(a) Alternative Parameters for Inner Shell Analysis of the End-121[a]

	R (Å)	$2\sigma^2$ (Å^2)	FI	R (%)
(i)				
2N	1.93	0.013		
1S	2.13	0.000	0.94	31.7
(ii)				
2N	1.92	0.004		
1S	2.15	0.001	1.06	32.4
(iii)				
1N	1.88	–0.007		
1N	2.14	0.049		
1S	2.14	–0.004	0.86	30.9
(iv)				
1N	1.88	–0.008		
1N	2.11	–0.008		
1S	2.13	–0.007	0.87	31.0
(v)				
1N	1.88	0.004		
1N	2.00	0.004		
1S	2.13	0.001	0.95	31.6
(vi)				
2N	1.93	0.004		
1S	2.16	0.001		
1O	2.26	0.008	0.83	30.6

(b) Final Fit Parameters for End-121 EXAFS, Including the Oxygen Shell at 2.26 Å[b,c]

shell	atoms	R (Å)	$2\sigma^2$ (Å^2)	shell	atoms	R (Å)	$2\sigma^2$ (Å^2)
1	2N	**1.93**	**0.004**	6	2N	4.12	0.015
2	1S	**2.15**	**0.001**	7	1O	**2.83**	**0.020**
3	2C	2.86	**0.007**	8	1O	**2.26**	**0.013**
4	2C	3.01	0.007	9	2C	**3.26**	**0.012**
5	2C	4.02	**0.015**				

[a] The first shell of the End-121 mutant was fitted using the raw EXAFS spectrum (i.e., not Fourier filtered data) between k = 3.6 and 11.2 Å^{-1}: (i) 2N + 1S model, both R and $2\sigma^2$ refined; (ii) 2N + 1S model, R refined, $2\sigma^2$ fixed; (iii) 1N + 1N + 1S model, both R and $2\sigma^2$ refined; (iv) 1N + 1N + 1S model, R refined, $2\sigma^2$ refined with constraint $2\sigma^2$(N1) = $2\sigma^2$(N2); (v) 1N + 1N + 1S model, R refined, $2\sigma^2$ fixed; (vi) 2N + 1S + 1O model, both R and $2\sigma^2$ refined. [b] Refined parameters are given in bold. [c] E_o = 20.97; $2\sigma^2$ is the Debye–Waller factor; fit index = 0.14; R factor = 11.9%.

carbonyl oxygen of Gly-45 and the α-carbon of the residue at position 121 varies very little in the mutant proteins compared to the wild-type protein. A simple modeling study using crystallographic data of the wild-type protein indicates that, in the Asp-121 mutant, the aspartic acid residue is too short to reach copper unless some movement in the copper pocket takes place. Also, the gap between the carboxylate group and the metal is not large enough to accommodate a water molecule unless the side chain is pointing away from the copper. On the other hand, this type of flexibility in the Cu cavity does exist as it is now known that much larger residues can be accommodated. For example, the mutants Met121Phe and Met121Trp display the properties of a type 1 copper site (Karlsson et al., 1991). In the case of the End-121 mutant, the space created by the absence of the methionine can be filled by the bulk solvent. This model is sketched in Figure 8a. However, we note that the methionine-121 in Az_p is not directly exposed to the bulk solvent.

At pH 5 the water molecule is probably hydrogen bonded to the Asp-121 carboxylate group, preventing a strong oxygen to metal interaction. At pH 8 the carboxylate group has titrated, giving rise to a stronger oxygen to copper interaction. This model is sketched in Figure 8b. The difference in water interaction at low and high pH is then largely responsible for the spectral changes in the visible and EPR spectra. The presence of the carboxylate group and hydrogen bonds,

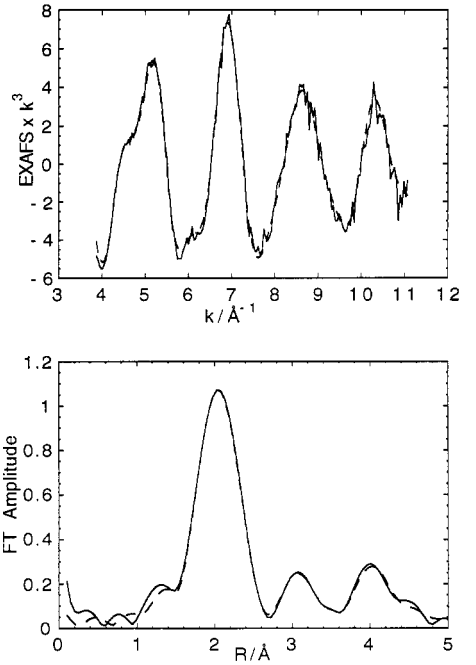

FIGURE 6: EXAFS data for the End-121 mutant with the basic model [i.e., two imidazole + one S(Cys)] an O at 2.26 Å, another oxygen at 2.83 Å, and two C atoms at 3.26 Å.

however, put some constraints on the mobility of the water molecule, and it is not as free as in the End-121 mutant.

In the End-121 mutant, on the other hand, the water molecule is at approximately the same distance from the metal ion, but the absence of the last eight residues of the protein probably makes the protein structure less rigid. In this case the constraints on the water molecule are more relaxed so that it could adopt a conformation, relative to copper, in which the Cu(II) form is preferentially stabilized. This would in turn lower the reduction potential of the copper site, and the reduction potential is indeed the lowest we have found in any Met-121 azurin mutant (Pascher et al., 1992).

In this model, the interpretation of the EXAFS data would then be that the oxygen at ~2.25 Å is a water molecule and the oxygen at ~2.8 Å is the carbonyl oxygen from Gly-45 (Figure 8a,b).

The above assignment for the oxygen shells requires spaces near the methionine pocket in order to accommodate a water molecule. The alternative assignment is shown in Figure 8c,d, in which the Gly-45 moves and in the Asp-121 mutant, the aspartate coordinates directly to the copper at pH 8.

For the Asp-121 mutant, a molecular modeling study, using the crystallographic coordinates of Az_p (Adman and Hasnain, unpublished data to 2.7-Å resolution refined to R = 20%), suggests that aspartic acid can be accommodated at the Cu site without requiring any significant change in the structure of the protein. On this basis, the Cu–O distance for Asp-121 mutant would be expected to be ~3.2 Å, with the equivalent distance of the Glu-121 and Lys-121 mutants at 2.4 and 2 Å, respectively (Karlsson et al., 1991). The molecular modeling distance of 3.2 Å for O(Asp) is closer to the observed Cu–O distance of 2.88 Å. Thus, the 2.88-Å O shell could originate from the aspartic acid residue in the Asp-121 protein. In this case, molecular modeling suggests that there is no room for a water molecule at ~2.25 Å from the copper. Consequently, the 2.25-Å shell is assigned to the Gly-45. We note that there are no geometrical constraints which would prevent Gly-45 from approaching Cu and getting as close as this. Recently, the crystal structure of a heterologously expressed Zn azurin

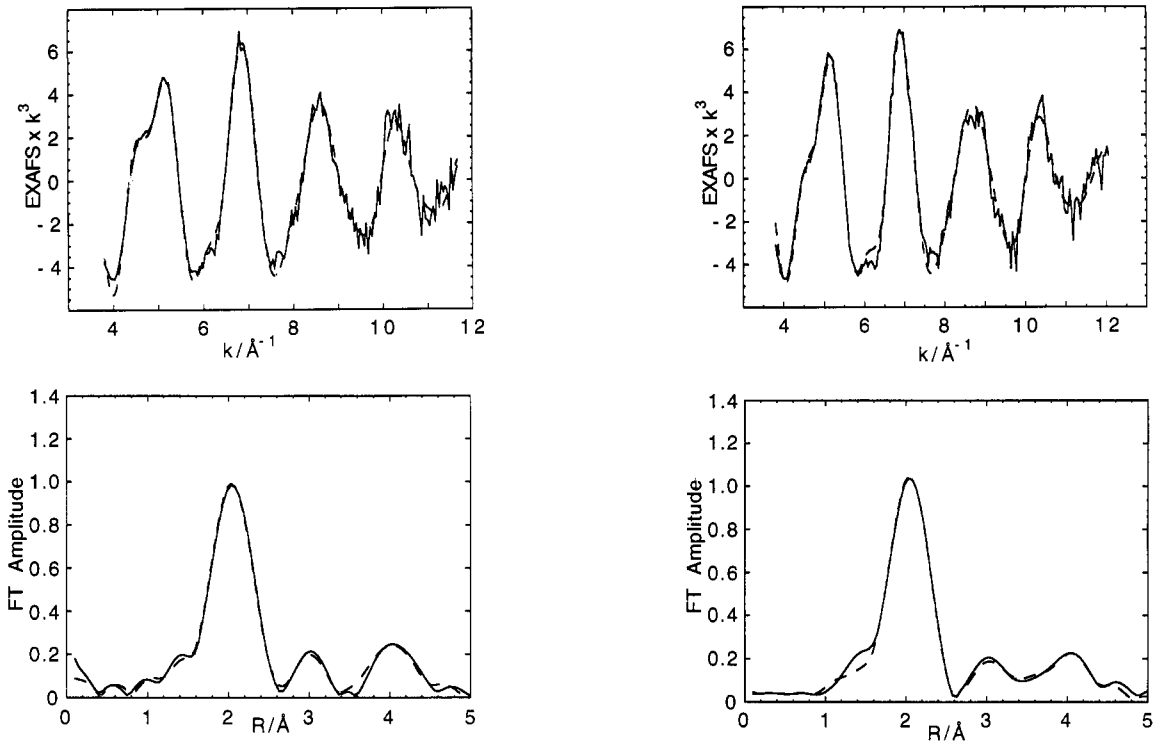

FIGURE 7: (a, left panels) Simulation for Asp-121 EXAFS at pH 8.0 with a model essentially similar to that obtained for the End-121 mutant incouding the short Cu–O shell at 2.23 Å. (b, right panels) Simulation of Asp-121 EXAFS at pH 5.0.

Table V. EXAFS Parameters for (a) Asp-121 at pH 8.0 and (b) Asp-121 at pH 5.0

shell	atoms	R (Å)	$2\sigma^2$ (Å^2)	shell	atoms	R (Å)	$2\sigma^2$ (Å^2)
(a) Parameters Used To Fit Cu K-Edge EXAFS of Asp-121 pH 8.0[a]							
1	2N	1.93	0.006	6	2N	4.12	0.015
2	1S	2.16	0.001	7	1O	2.88	0.023
3	2C	2.86	0.009	8	1O	2.23	0.016
4	2C	3.00	0.009	9	2C	3.28	0.020
5	2C	4.03	0.015				
(b) Parameters Used To Fit Cu K-Edge EXAFS of Asp-121 pH 5.0[b]							
1	2N	1.93	0.006	6	2N	4.15	0.015
2	1S	2.15	0.003	7	1O	2.88	0.050
3	2C	2.85	0.008	8	1O	2.26	0.012
4	2C	3.00	0.008	9	2C	3.26	0.010
5	2C	4.02	0.015				

[a] E_o = 18.8; $2\sigma^2$ is the Debye–Waller factor; fit index = 0.22; R factor = 14.8%. [b] E_o = 18.8; $2\sigma^2$ is the Debye–Waller factor; fit index = 0.21; R factor = 15.4%.

has been determined (Nar et al., 1992) which shows that Gly-45 is able to move significantly. In this case, O(Gly-45) has moved by 0.3 Å, which along with other small adjustments, brings the Gly-45 oxygen as close as 2.32 Å from Zn. Baker et al. (1991) has found similar movement of carbonyl oxygen in the Cd(II) derivative of *A. denitrificans* azurin, where the Cd–O distance has been determined to be ~2.6 Å.

This alternative assignment of the oxygen shells therefore has the O at ~2.25 Å in both mutants as originating from the Gly-45 and the O at ~2.8 Å arising from water (in End-121, Figure 8c) or carboxylate (in Asp-121, Figure 8d). This interpretation is tempting as it provides a neat rationalization of several other observations. For example, no significant change in EXAFS has been observed for the Asp-121 mutant as a function of pH other than an increased α for the Cu–S(Cys) bond and the absence of long (2.88 Å) Cu–O bond at pH 5.0. Thus, protonation/deprotonation of Asp-121 would directly yield to spectral changes, and at the same time the ligand would become invisible by EXAFS, either because it has moved away or has become much more delocalized. In the case of the End-121 mutant, the lack of a pH dependence in the spectroscopic properties and the observation of a Cu–O distance of ~2.25 Å are also consistent with this rationale. This interpretation is also interesting in that the O from Gly-45 perhaps is the key difference in providing greater stability of the azurin methionine mutants compared to that in plastocyanin-type sequences, where carbonyl oxygen is constrained from approaching Cu by being part of a rather short loop (Adman, 1985).

There are several additional observations which need discussion in the light of above possibilities. Table VII summarizes a number of these observations and is presented here to facilitate the discussion.

Spectroscopic Properties. The first point to note is the correlation present in Table VII between some of the spectroscopic characteristics. The proteins can be grouped according to their EPR and electronic absorption spectra: proteins with axial EPR have weaker electronic absorption at ca. 450 nm, stronger absorption at ca. 780 nm, and longer λ_{max} (≥620 nm) than proteins with rhombic EPR. There is one exception to this trend given in Table VII, and that is plastocyanin (from spinach leaves, Pc_s), which has axial EPR and λ_{max} = 600nm. The order in which the 628-nm band shifts to higher energy is

$$Az_p(628\ nm) > Az_a > Asp(pH\ 5.0) > End > Asp(pH\ 8.0) > St(pH\ 7.0) > Pc_s > Ru > St\ pH\ 11.0\ (588\ nm)$$

The major contribution to the ca. 628-nm band arises from the S(Cys)$\sigma \rightarrow Cu(d_{x^2-y^2})$ transition. Both azurin and plastocyanin have "similar" Cu–S(Cys) bonds distances (in crystallographic terms). The difference in electron density on the Cu has therefore been attributed to a weaker axial interaction from S(Met) in azurin compared to plastocyanin (Ainscough et al., 1987). An additional interaction of Cu with the long distance to the peptide oxygen from Gly-45 has

Table VI: Cu Coordination in Azurin and Mutants and Their Comparison with the Crystallograhic Data[a]

	crystallographic[b]			XAFS			
						Asp-121	
	Az_p (pH 9)	Az_a	Pc_p	Az_p (pH 8)	End-121	pH 8	pH 5
Cu–S (Cys)	2.25	2.14	2.13	2.12	2.15	2.16	2.15
				(0.000)	(0.001)	(0.001)	(0.003)
Cu–N (His)	2.03	2.00	2.10	1.92	1.93	1.93	1.93
	2.11	2.08	2.04	1.92	1.93	1.93	1.93
				(0.005)	(0.004)	(0.006)	(0.006)
Cu–O[c]	2.97	3.13	3.82	2.79	2.83	2.88	–
				(0.014)	(0.020)	(0.023)	–
Cu–S (Met)	3.15	3.11	2.90	3.04[d]	–	–	–
Cu–C[e]	–	–	–	3.26	3.26	3.28	3.26
				(0.014)	(0.012)	(0.020)	(0.010)
Cu–O[f]					2.26	2.23	2.26
					(0.013)	(0.016)	(0.012)

[a] Distances are in Å; numbers in parentheses are Debye–Waller terms ($2\sigma^2$) in Å^2. [b] As summarized in Nar et al. (1991). [c] Glycine in Az_a, Az_p, and proline in the case of Pc_p. [d] The Cu–S(Met) back-scattering is not determined unambiguously by EXAFS. [e] Several C atoms are present between ca. 3.2 and 3.6 Å in the crystal structures from the histidine and cysteine side chains. [f] Assignment of this O can be exchanged for the glycine O (see Discussion).

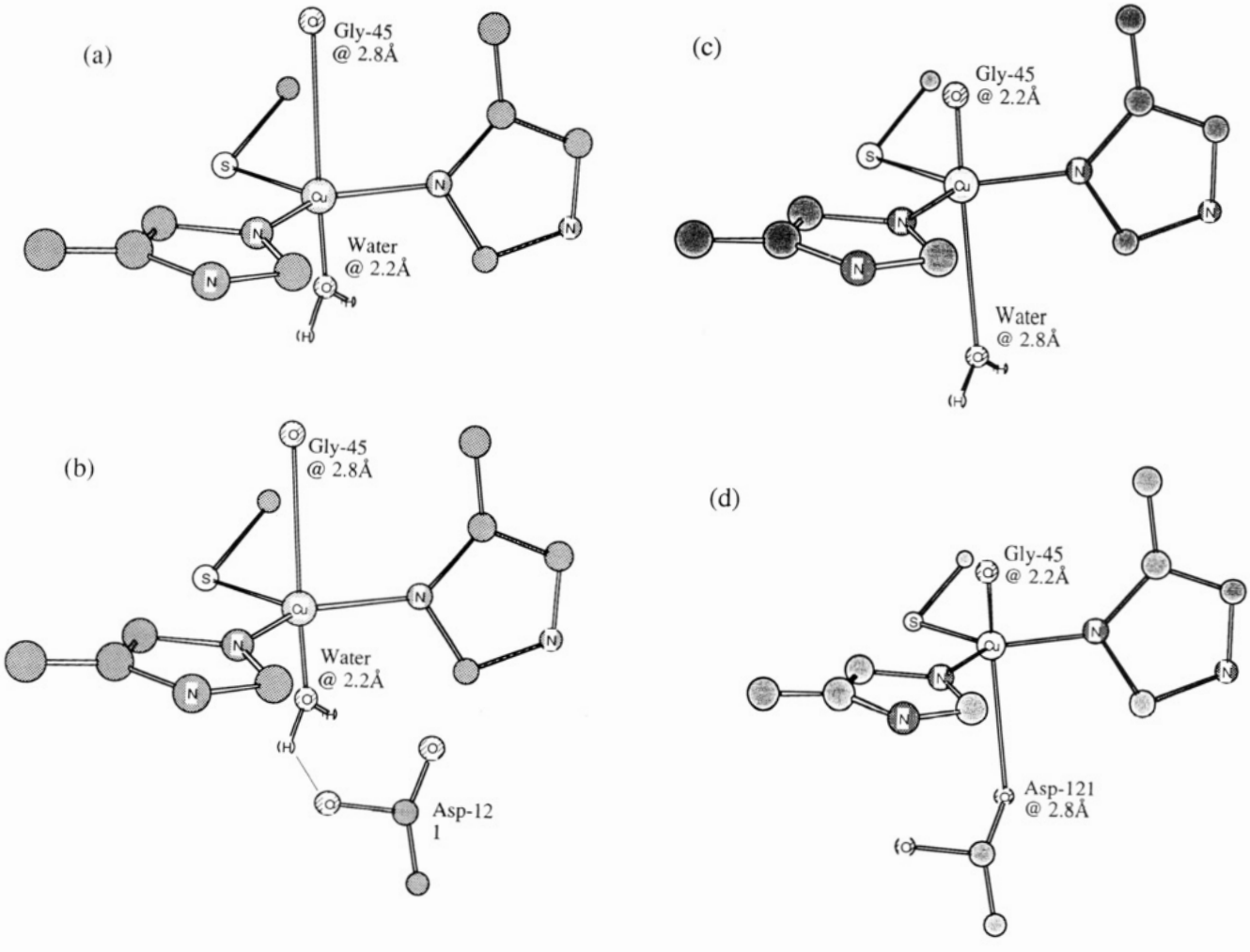

FIGURE 8: Schematic of the copper site in the azurin mutants showing the possible structural interpretations of the spectroscopic data. In (a) End-121 and (b) Asp-121, a water is coordinated at ~2.25 Å, with the Gly-45 oxygen at ~2.8 Å. In (c) End-121 and (d) Asp-121, the Gly-45 oxygen is at ~2.25 Å, with the ~2.8-Å oxygen being from either water or the aspartic acid, respectively.

also been suggested as a possibility for the observed differences. Thus, the difference between plastocyanin and Az_a may be rationalized by a weaker methionine interaction and a stronger O_{45} interaction, while the difference between Az_a and Az_p is rationalized by a stronger interaction of O_{45} in the case of Az_p. In addition, the nature of residue "X" (X refers to Met or its replacement) appears to play a role. Karlsson et al. (1991) have noted that methionine mutants of azurin can be grouped together, with polar and hydrophobic residues at position 121 displaying clearly different spectroscopic properties. Solomon and his co-workers (Gewirth et al., 1987) have shown using X_α calculations that the spectral properties of the plastocyanin site can be modified to stellacyanin by increasing the strength of the axial interaction from group "X" and reducing the site symmetry from C_{3v} to C_{2v}. Thus, changes in the spectral properties may arise as a direct result

Table VII: Basic Spectroscopic Properties of Azurin and the Asp-121 and End-121 Mutants Compared with Other Type 1 Copper Proteins[a]

protein[b]	S(Met)	long O[c]	ESR	λ_{max} (nm)	λ_{780} (nm)	λ_{450} (nm)	E^0 (mV)
Pc_s (7.0)[d]	√	×	axial	600	strong	weak	370
Az_a (7.0)[e]	√	√	axial	620	strong	weak	276
Az_p (8.0)	√	√	axial	628	strong	weak	293
Az_p (5.0)	√	√	axial	628	strong	weak	346
Asp (5.0)	×	×	axial	620	strong	weak	327
Asp (8.0)	×	√	rhombic	612	weak	strong	287
End (7.0)	×	√	rhombic	616	weak	strong	205
End (5.0)	×	√	rhombic	616	weak	strong	
St (7.0)[f]	×	√[g]	rhombic	604	weak	strong	184
Ru (3.2)[h]	√	?	rhombic	590	weak	strong	680

[a] The symbols √ and × in the columns for "S(met)" and "long O" signify the presence or absence, respectively, of these ligands at the Cu site. For example, for native plastocyanin and azurin, and probably for rusticyanin, the S(met) ligand is present (√); in the mutant azurins and in stellacyanin, the S(met) is absent (×). These two columns are included to summarize the results and discussion given in the text. [b] Numbers in parentheses are pH values. Spectroscopic data are taken from the references indicated in footnotes *d–f* and *h*. [c] The "long O" refers to the possibility of a Cu–O shell at ~2.8 Å (see the text for details). [d] Katoh et al. (1962); Pc_s is spinach plastocyanin. [e] Ainscough et al. (1987). [f] Reinhammar (1972). [g] Unpublished results. [h] Ingledew and Cobley (1980).

of these axial interactions or due to the change in site symmetry which these interactions may bring. The observation of a close O shell ca. 2.25 Å in the mutants does not seem to have an obvious effect on the spectroscopic properties displayed by the mutants, and it would be of interest to calculate the electronic structure of the Cu site in these cases. It is possible that the spectral properties of the Cu site is dominated by the site symmetry imposed by the two histidine and the cysteine ligands.

The change in the ca. 628-nm band with pH for Asp-121 points to a decrease in electron density on Cu at low pH. Note that the shift to shorter λ in the 628–600-nm absorption region when moving to a higher pH is a trend noticed in several type 1 Cu containing proteins, such as Az_a, St, tree laccase, mavicyanin, and umecyanin [see the references in Ainscough et al. (1987)]. In Az_a this shift is accompanied by a shift in the 460-nm band to 452 nm. However, in these cases there is no corresponding change from axial to rhombic EPR. The decrease in S(Cys)$\sigma \rightarrow$ Cu($d_{x^2-y^2}$) charge transfer may be explained by the protonation/deprotonation of the polar aspartate group at low/high pH. At low pH less charge is transferred to copper from aspartate, resulting in a lower S(Cys)$\sigma \rightarrow$ Cu($d_{x^2-y^2}$) charge transfer. EXAFS shows that the Cu–S(Cys) distance is the same at both pH 5.0 and 8.0 in Asp-121. However, α is larger at pH 5.0 (0.003 Å^2 compared to 0.001 Å^2 at pH 8.0). Even though α, the Debye–Waller factor, is a sum of both the static and thermal disorder, the increased value at low pH reflects a delocalization of the bond and is equivalent to a reduced electronic overlap between the Cu and S orbitals. In view of Solomon's calculations, the changes in the Cu–S(Cys) interaction would be marked if the Asp group was in the axial position and site symmetry could change (Gerwith & Solomon, 1988).

Reduction Potentials. The End-121 mutant shows a reduction potential similar to St while the Asp-121 mutant shows a potential similar to Az_p with the high-pH form showing a potential 40 mV lower than the low-pH form. However, no Met-121 mutant of Az_p shows a reduction potential similar to that of rusticyanin. In view of the near constancy of the three strongly bound ligands (the two His and a Cys) among the blue Cu proteins, it has been suggested that it is the axial ligands and variation in them which tunes the reduction potentials (Gray & Malmström, 1983). Both the polarity and charge of the axial group (and thus its distance) are likely to be important. The close similarity of the EXAFS spectrum for End-121 and Asp-121 (pH 8.0) and a higher reduction potential of the Asp-121 mutant (an increase of 80 mV over the End-121 mutant) reflects the importance of the nature of the residue in the Met-121 position. The polar nature of the Asp-121 residue can be directly ascribed to the difference in the reduction potential for the two mutants. The pH dependence of the reduction potential for Asp-121 could directly result from the protonation/deprotonation of the aspartic acid residue itself; alternatively, the decrease of the potential of Asp-121 at high pH could be due to a titrating group other than the aspartic acid. Nar et al. (1991) suggest that, in the case of wild-type Az_p, the pH-dependent redox change is due to the deprotonation of His-35 which induces a Pro-36–Gly-37 main chain peptide bond flip and removes positive charge from Cu. However, similar pH-dependent redox changes have been observed for His-35 mutants (Pascher, 1992). The pK_a of 6.2 for this group in the oxidized wild-type protein is the same as we observe for the Asp-121 mutant. The similarity in the pH dependence of the reduction potential for the wild-type and Asp-121 mutant could then be explained by a smaller difference in the pK_a (ox) and the pK_a (red) for the Asp residue. The low reduction potential of the End-121 mutant may arise from the high polarizibility of the water molecule (present at either at 2.26 or 2.83 Å) and a site more suited for Cu(II).

CONCLUSION

The XAFS and spectrochemical studies reported here for azurin and some of the methionine mutants show that both the spectral and redox properties of the Cu(II) center in azurin can be modified substantially by a single mutation. Even though the methionine ligand is not essential for producing a blue copper site, the Cu center is sensitive to the ligand which occupies this place. In mutants where the mutated residue is absent (End-121) or is shorter than the methionine residue (Asp-121), and is therefore unlikely to coordinate to copper, the carbonyl O from Gly-45 may move closer in and thus stabilize the Cu(II) oxidation state, as suggested by one of the possibilities for the O shell at ~2.25 Å. On the other hand, the possibility that this shell is a water ligand cannot be ruled out in the present work. A recent study on electronic absorption spectra for several mutants with different metals suggests that the metal site in the methionine mutants of azurin is more flexible than that in native azurin (Di Billio et al., 1992). It is evident from this and other work on azurin mutants that the Cu site is not rigid but should be considered as "responsive", one which is able to react to changes in the ligands, pH, oxidation state, and even other metals. The presence of methionine may thus be seen as a constraint for Cu to adopt its preferred Cu(II) coordination, thus facilitating the redox role of Cu in these proteins by providing an

environment easily adaptable for both the Cu(II) and Cu(I) oxidation states.

ACKNOWLEDGMENT

We thank Professors Bo G. Malmstrom, Tore Vanngard and Elinor Adman for their helpful comments and useful discussion.

REFERENCES

Adman, E. T. (1985) in *Topics in Molecular and Structural Biology: Metalloproteins* (Harrison, P., Ed.) Vol. I., pp 1–42, Verlag Chemie, Weinheim.

Adman, E. T. (1991) in *Advances in Protein Chemistry* (Anfinsen, C. B., Edsall, J. T., Richards, F. M., & Eisenberg, D. S., Eds.) Vol. 42, pp 145–197, Academic Press, London.

Adman, E. T., & Jensen, L. H. (1981) *Isr. J. Chem. 21*, 8–12.

Adman, E. T., Stenkamp, R. E., Sieker, L. C., & Jensen, L. H. (1978) *J. Mol. Biol. 123*, 35.

Ainscough, E. W., Bingham, A. G., Brodie, A. M., Ellis, W. R., Gray, H. B., Loehr, T. M., Plowman, J. E., Norris, G. E., & Baker, E. N. (1987) *Biochemistry 26*, 71–82.

Baker, E. N. (1988) *J. Mol. Biol. 203*, 1071–1075.

Baker, E. N., Anderson, B. F., Blackwell, K. E., Kingston, R. L., Norris, G. E., & Shepard, W. E. B. (1991) *J. Inorg. Biochem. 43*, 162.

Bergman, C., Gandvik, E.-K., Nyman, P. O., & Strid, L. (1977) *Biochem. Biophys. Res. Commun. 77*, 1052–1059.

Binsted, N., Cook, S. L., Evans, J., Greaves, G. N., & Price, R. J. (1987) *J. Am. Chem. Soc. 109*, 3669–3676.

Binsted, N., Gurman, S. J., Campbell, J. W., & Stephenson, P. (1991) SERC Daresbury Laboratory Program EXCURVE, Warrington, U.K.

Binsted, N., Strange, R. W., & Hasnain, S. S. (1992) *Biochemistry 31*, 12117–12125; also Daresbury Laboratory Preprint DL/SCI/p792E.

Blackburn, N. J., Strange, R. W., Farooq, A., Haka, M. S., & Karlin, K. D. (1988) *J. Am. Chem. Soc. 110*, 4263–4272.

Collyer, C. A., Guss, J. M., Sigimura, Y., Yoshizaki, F., & Freeman, H. C. (1990) *J. Mol. Biol. 211*, 617–632.

Di Billio, A. J., Chang, T. K., Malmstrom, B. G., Gray, H. B., Karlsson, B. G., Nordling, M., Pascher, T., & Lundberg, L. G. (1992) *Inorg. Chim. Acta 198–200*, 145–148.

Ellis, W. L. (1986) Ph.D. Thesis, California Institute of Technology, Pasedena, CA.

Gerwith, A. A., Cohen, S. L., Schugar, H. J., & Solomon, E. I. (1987) *Inorg. Chem. 26*, 1133–1146.

Gray, H. B., & Malmström, B. G. (1983) *Comments Inorg. Chem. 2*, 203–209.

Groeneveld, C. M., Feiters, M. C., Hasnain, S. S., Van Rijn, J., Reedijk, J., & Canters, G. W. (1986) *Biochim. Biophys. Acta 873*, 214–227.

Gurman, S. J., Binsted, N., & Ross, I. (1984) *J. Phys. C: Solid State Phys. 17*, 287–290.

Gurman, S. J., Binsted, N., & Ross, I. (1986) *J. Phys. C: Solid State Phys. 19*, 1845–1861.

Guss, J. M., & Freeman, H. C. (1983) *J. Mol. Biol. 169*, 521–563.

Guss, J. M., Harrowell, P. R., Murata, M., Norris, V. A., & Freeman, H. C. (1986) *J. Mol. Biol. 192*, 361–387.

Hahn, J. E., Scott, R. A., Hodgson, K. O., Doniach, S., Desjardins, S. E., & Solomon, E. I. (1982) *Chem. Phys. Lett. 88*, 595.

Hasnain, S. S., Ed. (1991) *X-ray Absorption Fine Structure*, Ellis Horwood Ltd., Chichester, U.K.

Hasnain, S. S., & Strange, R. W. (1988) in *Biophysics and Synchrotron Radiation* (Hasnain, S. S., Ed.) pp 104–122, Ellis Horwood Ltd., Chichester, U.K.

Heineman, W. R., Norris, B. J., & Goelz, J. F. (1975) *Anal. Chem. 47*, 79–84.

Ingledew, W. J., & Cobley, J. G. (1980) *Biochim. Biophys. Acta 590*, 141–158.

Karlsson, B. G., Pascher, T., Nordling, M., Arvidsson, R. H. A., & Lundberg, L. G. (1989) *FEBS Lett. 246*, 211–217.

Karlsson, B. G., Nordling, M., Pascher, T., Tsai, L.-C., Sjolin, L., & Lundberg, L. G. (1991) *Protein Eng. 4*, 343–349.

Katoh, S., Shiratori, I., & Takimaya, S. (1962) *J. Biochem. (Tokyo) 51*, 32–39.

Lommen, A., Pandya, K. I., Koningsberger, D. C., & Canters, G. W. (1991) *Biochim. Biophys. Acta 1076*, 439–447.

Malmström, B. G. (1965) in *Oxidases and Related Systems* (King, T. E., et al., Eds.) pp 207–221, John Wiley & Sons, New York.

Morrell, C., Baines, J. T. M., Campbell, J. W., Diakun, G. P., Dobson, B. R., Greaves, G. N., & Hasnain, S. S. (1989) *EXAFS Users Manual*, Daresbury Laboratory, Warrington, U.K.

Nar, H., Messerschmidt, A., Huber, R., van de Kamp, M., & Canters, G. W. (1991) *J. Mol. Biol. 221*, 765–772.

Nar, H., Huber, R., Messerschmidt, A., Filippou, A. C., Barth, M., Jaquind, M., van de Kamp, M., & Canters, G. W. (1992) *Eur. J. Biochem. 205*, 1123–1129.

Norris, G. E., Anderson, B. F., & Baker, E. N. (1986) *J. Am. Chem. Soc. 108*, 2784–2785.

Parr, S. R., Barber, D., Greenwood, C., Phillips, B. W., & Melling, J. (1976) *Biochem. J. 157*, 423–430.

Pascher, T. (1992) Ph.D. Thesis, University of Göteborg, Sweden.

Penner-Hahn, J. E., Murata, M., Hodgson, K. O., & Freeman, H. C. (1989) *Inorg. Chem. 28*, 1826–1832.

Reinhammar, B. (1972) *Biochim. Biophys. Acta 275*, 245–259.

Reinhammar, B. (1979) in *Advances in Inorganic Biochemistry*, pp 92–118, Elsevier/North Holland, Amsterdam.

Ryden, L. (1984) in *Copper Proteins and Copper Enzymes* (Lontie, R., Ed.) Vol. I, pp 157–182, CRC Press, Boca Raton, FL.

Salusita, N., Anson, F. C., & Gray, H. B. (1979) *J. Am. Chem. Soc. 101*, 455–458.

Schulman, R. G., Yafet, T., Eisenberger, P., & Blumberg, W. E. (1976) *Proc. Natl. Acad. Sci. U.S.A. 73*, 1384.

Scott, R. A., Hahn, J. E., Doniach, S., Freeman, H. C., & Hodgson, K. O. (1982) *J. Am. Chem. Soc. 104*, 5364–5369.

Strange, R. W., Blackburn, N. J., Knowles, P. F., & Hasnain, S. S. (1987) *J. Am. Chem. Soc. 109*, 7157–7162.

Tullius, T. D., Frank, P., & Hodgson, K. O. (1978) *Proc. Natl. Acad. Sci. U.S.A. 75*, 4069.

Urbaniczky, C. (1984) Ph.D. Thesis, Uppsala University, Uppsala, Sweden.

van de Kamp, M., Hali, F. C., Rosato, N., Finazzi Agro, A., & Canters, G. W. (1990) *Biochim. Biophys. Acta 1019*, 283–292.